# CHAPTER IV
# RESULTS AND DISCUSSION

## 4.1 Determination of Response Time Constant

The method for determining the response time constant, $\alpha_e$, is described in Figure A1. Equation (2.4) was used to find the value of this constant by fitting the equation with the experimental data using the Solver tool in Excel. The response time constants of the pH electrode at various mixing speeds (for batch operation) and various flow rates (for continuous operation) are shown in Tables 4.1 and 4.2. The plots of predicted and experimental concentrations of hydrogen ions are shown in Appendix A.

**Table 4.1** Summary of average values of response time constant of pH electrode for batch operation at various mixing speeds.

| **Mixing speed, rpm.** | **Response time constant, $sec^{-1}$** |
|---|---|
| 250 | 0.01493 |
| 500 | 0.02198 |
| 750 | 0.02456 |
| 1000 | 0.02580 |

Table 4.1 shows the response time constant at various mixing speeds (250, 500, 750 and 1000 rpm). The higher the mixing speed, the lower the response time. In other words, a higher mixing speed is more efficient for measuring the pH value of the solution. The result can be explained by considering the effect of mixing speed on the thickness of the stagnant liquid layer which normally exists near the surface of the probe. Thus, the higher the

mixing speed, the lower the thickness of the film, which promotes diffusion of $H^+$ ions into the inner core of the pH probe. It is also interesting to note that when the mixing speed is changed from 750 to 1000 rpm, the value of response time constant changes by only a small amount. It shows that at a mixing speed of 750 rpm, the film diffusion step is overcome.

**Table 4.2** Summary of response time constant of pH electrode for continuous operation at various flow rates of HCl solution.

| **Flow rate of HCl , ml/min** | **Response time constant, $sec^{-1}$** |
|---|---|
| 100 | 0.0130 |
| 150 | 0.0152 |
| 170 | 0.0159 |
| 200 | 0.0164 |
| 220 | 0.0164 |
| 240 | 0.0168 |

Table 4.2 shows the response time constant at various flow rates of 0.2 N HCl (100, 150, 170, 200, 220 and 240 ml/min). Again, the lower response time was achieved at the higher flow rates, which leads to a faster detection of the pH value of the solution. The same reason as in the case of batch operation can be used to describe the results.

When increasing the flow rate from 220 to 240 ml/min, the response time constant is nearly the same. It means that the effects of both film diffusion and the distance that the solution travels to meet the pH electrode have vanished. Therefore the real response time constant of the pH electrode in the case of continuous system equals to 0.0164 $sec^{-1}$.

From the results of both the batch and continuous operations, the response time of the pH electrode is about 100-150 sec (the calculations of the response time of pH electrode were shown in Appendix A), which is too high for accurate measurements. Namely, it is impossible to measure adsorption rates that occur roughly within 10-20 sec with a pH electrode that takes 100-150 sec to respond. Thus the new technique was employed by taking samples manually every 15-20 sec and then the pH value of each sample was measured accurately by allowing the pH values to reach equilibrium (see sections 3.3.2 and 3.3.3).

## 4.2 Batch Adsorption

A series of batch adsorption experiments was carried out in order to develop

1. A relationship between the concentrations of metal ions on the resin and in the solution at equilibrium ($q^e$ and $c^e$).
2. An expression for the rate of adsorption.

The initial concentration of $CaCl_2$ was varied from 0.05 to 0.4 N. From four sets of experiments shown in Figure 4.1, the relationship between $Ca^{2+}$ concentration on the resin and in the solution at equilibrium ($q^e$ and $c^e$) can be developed as shown in equation (4.1).

$$q^e = \beta (c^e)^{\frac{1}{n}} \qquad (4.1)$$

The relationship between ln $q^e$ and ln $c^e$ was plotted to find the constants β and n from the intercept and slope of the curve, respectively

(Figure 4.2). It was found that $\beta = 0.364$ and $n = 2.45$. From the shape the of the curve between q and t as shown in Figure 4.3 and because the rate of adsorption, dq/dt, must be equal to zero at equilibrium, the rate of adsorption should be of the form:

$$\frac{dq}{dt} = K\left(q^{e} - q\right) \qquad (4.2)$$

This rate of adsorption formula was validated by plotting ln $(1-q/q^{e})$ vs. time to find the rate constant K. If this rate of adsorption formula is valid, the values of K for all four sets of experiment should be the same (see Figure 4.4-4.7). From the results, the values of K for all four experiments are 0.1363, 0.1221, 0.1363 and 0.1312 $sec^{-1}$. Since the values agree well with each other, equation (4.2) is valid. This rate of adsorption was then used to predict the exit hydrogen ion for adsorption in fixed bed operation, where $q^{e}$ is defined by equation (4.1).

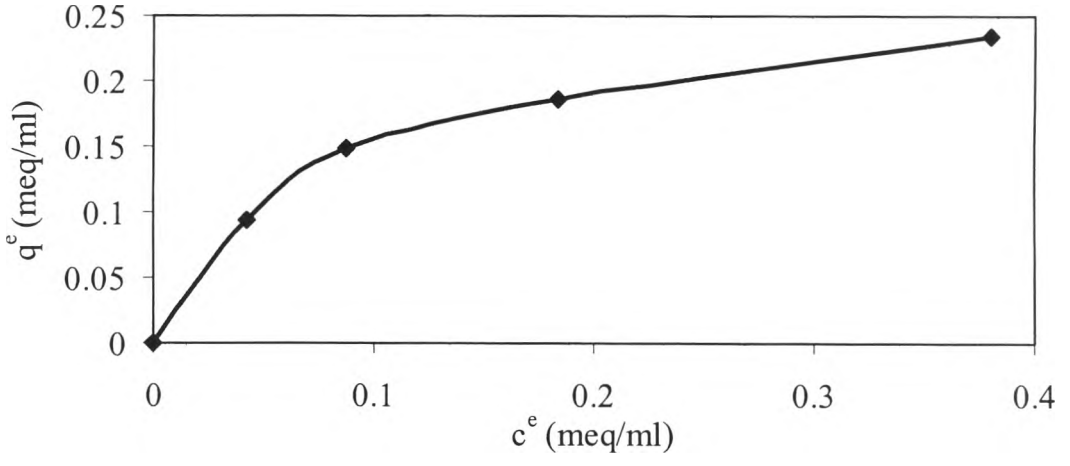


**Figure 4.1** Plot between equilibrium value of cation ion on the resin ($q^e$) and equilibrium concentration ($c^e$).

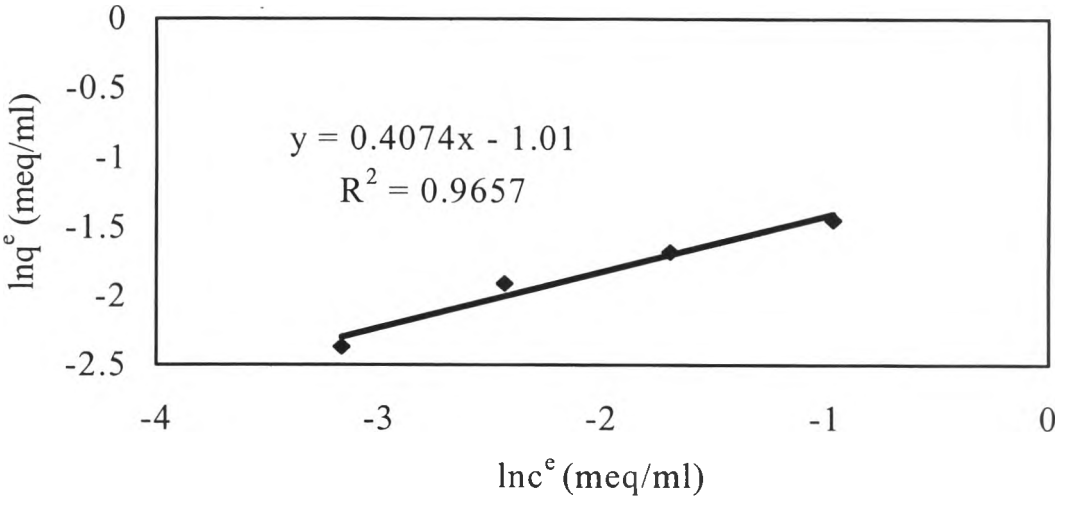


**Figure 4.2** Plot between natural log of equilibrium value of cation ion on the resin (ln $q^e$) and cation concentration in the solution (ln $c^e$) for four sets of experiments.

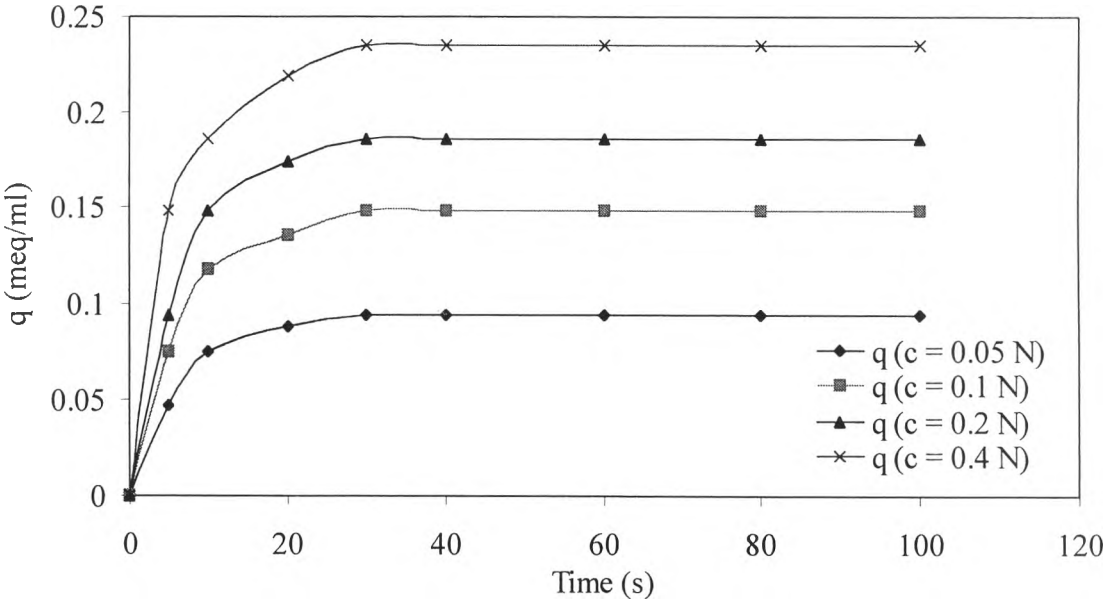


**Figure 4.3** Adsorption of calcium ion onto the resin with various initial concentrations as a function of time.

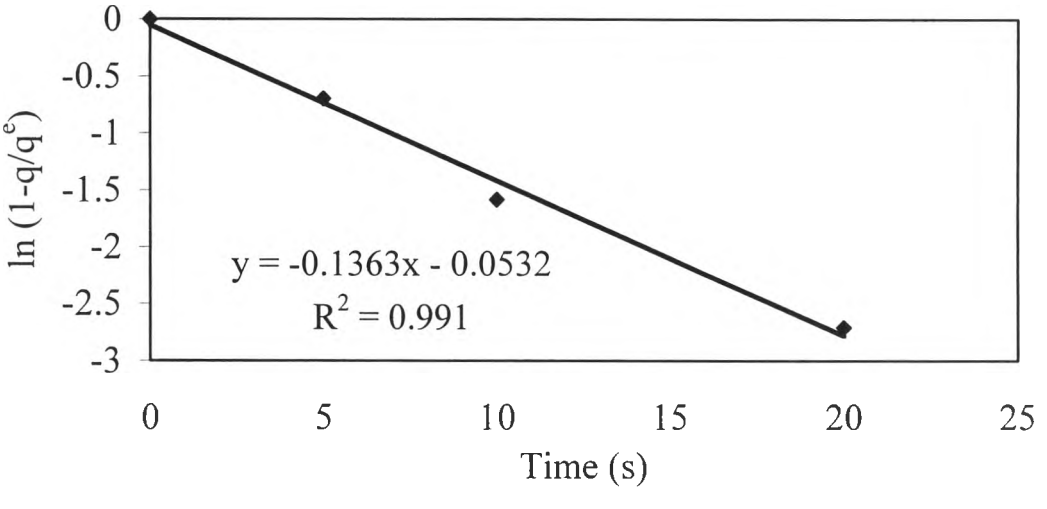


**Figure 4.4** Representation of relationship between ln ($1-q/q^e$) and time (initial concentration 0.05 N).

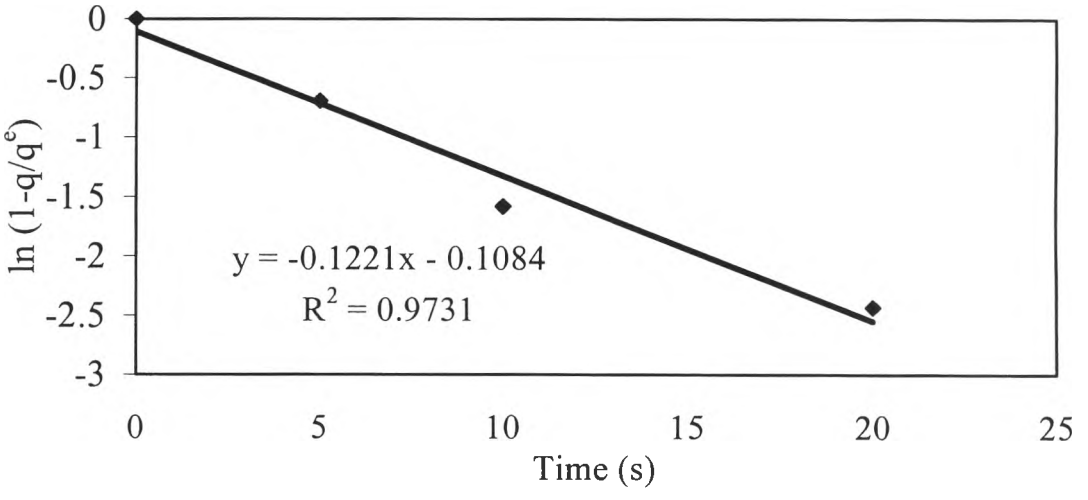


**Figure 4.5** Representation of relationship between ln $(1-q/q^e)$ and time (initial concentration 0.1 N).

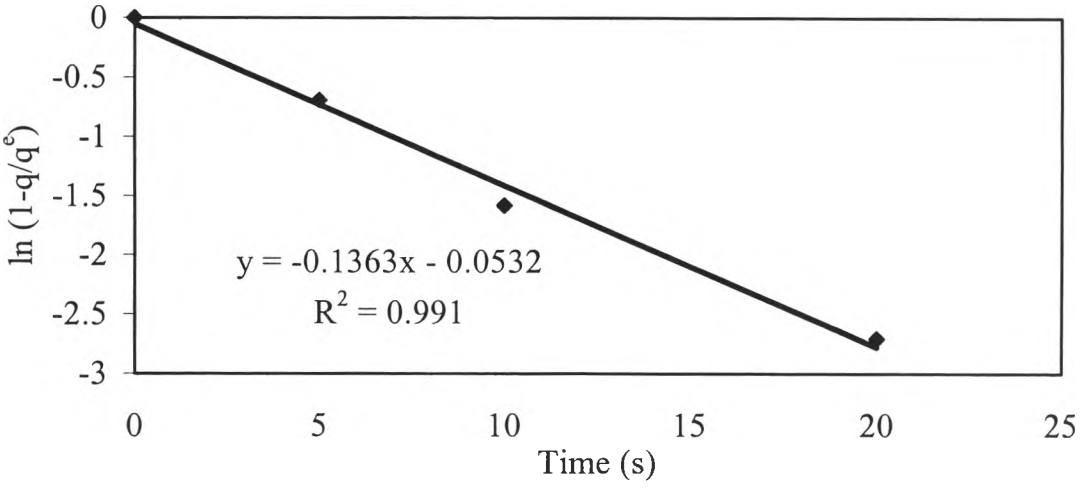


**Figure 4.6** Representation of relationship between ln $(1-q/q^e)$ and time (initial concentration 0.2 N).

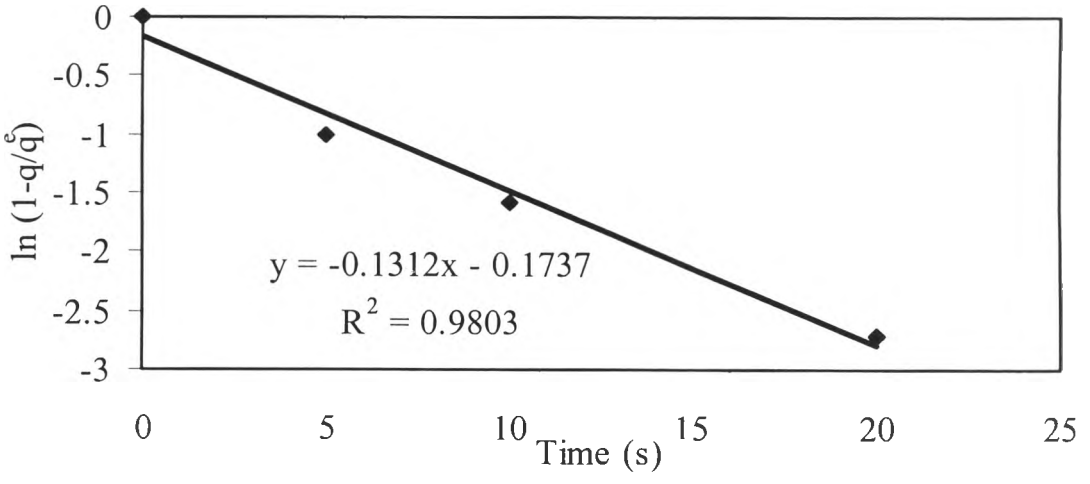


**Figure 4.7** Representation of relationship between ln $(1-q/q^e)$ and time (initial concentration 0.4 N).

## 4.3 No Adsorption Experiment

Figure 4.8 shows a comparison of the experimental data and the predicted data of the no-adsorption experiment modeled by using one CSTR and one ideal PFR in series. The schematic diagram of no adsorption with one CSTR and one ideal PFR in series was shown in Figure 2.2. The analytical solution of equation 2.16 was used with the incorporation of rate of adsorption equal to zero. The predicted values of calcium ion concentration in the solution, c, were converted to the concentration of hydrogen ion in the solution, h. The predicted values of hydrogen concentration were plotted against time and compared with the experimental data, as presented in Figure 4.8. The volume of the CSTR of 2.5 ml was obtained in this part and this value was further used in the fixed-bed adsorption part.

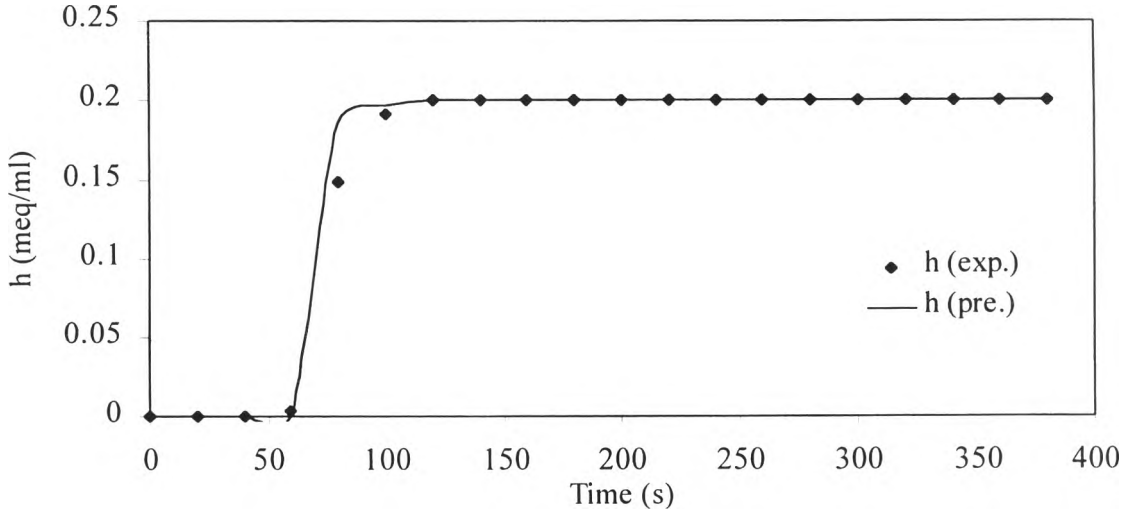


**Figure 4.8** The comparison of the experimental data and the predicted data of the no-adsorption test.

## 4.4 Adsorption Kinetics of Ion-Exchange Column with Downflow or Fixed-Bed Operation

Figure 4.9 shows a comparison of the predicted and the experimental hydrogen concentrations at the exit of the ion exchange column with downflow or fixed-bed operation. In Figure 4.9, $h_{mp}$ represents the predicted measured hydrogen ion concentration and $h_{me}$ represents the experimental data of measured hydrogen ion concentration. The adsorption in the fixed-bed operation or downflow direction depended upon both distance along the column, x, and time, t, so the *method of characteristics for hyperbolic equations* was used to solve the problem. Fortunately, this method can be simplified by using the *conventional finite-difference* method presented by equations (2.16) and (2.17) instead. Equations (2.16) and (2.17), together with a completely *implicit approach*, were used to predict the concentration of $Ca^{2+}$ ions in the solution, c, at any time t and length of column, x. A trigger cell was used to start the process by using the trigger cell and the logical function (how the trigger cell works and how it relates to the completely implicit method are described in Appendices E and C, respectively). The under-relaxation method was also used to protect the negative c value occurring in some step of iterations (how the under-relaxation works and how it relates to the completely implicit method are described in Appendices F and C, respectively). The volume of the CSTR found from the no-adsorption part was included in the mathematical model. Finally, from the exit q values predicted by the spreadsheet, the corresponding predicted exit value of h can be computed directly, and then be compared with the experimental exit h value as shown in Figure 4.9.

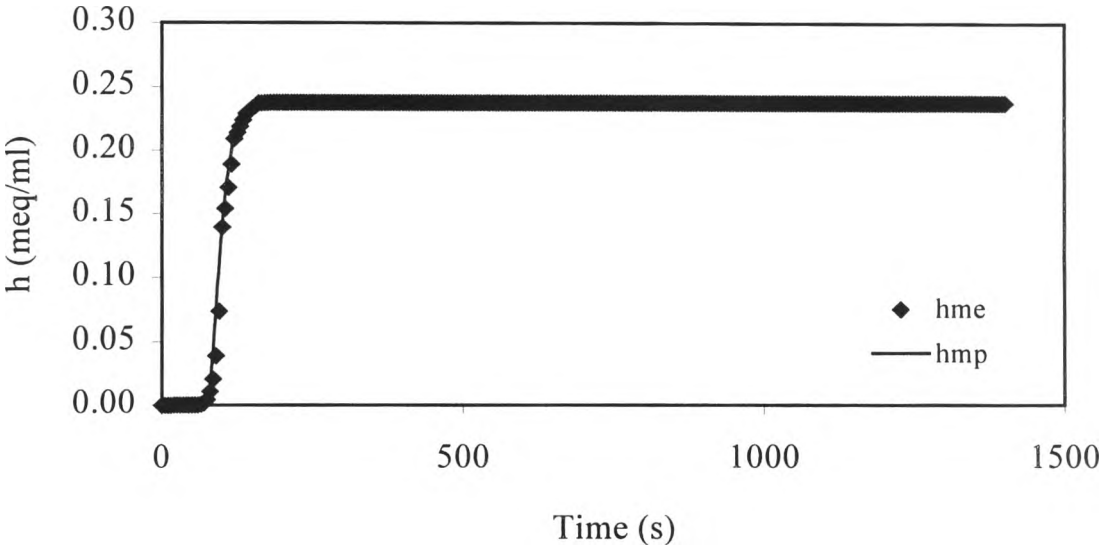


**Figure 4.9** The comparison of the experimental data and the predicted data for calcium ions at the column exit with fixed-bed operation.

## 4.5 Adsorption Kinetics of Mixed-Ion ($Ca^{2+}/Mg^{2+}$) System

The competitive adsorption of a mixed-ion system containing $Ca^{2+}$ and $Mg^{2+}$ was studied in both batch and fixed-bed (continuous) operations.

### 4.5.1 Batch Operation

The diagram of steps in determining the fraction of ion adsorbed onto the resins for batch operation is shown in Figure D1. The initial adsorption rate can be calculated from the initial slope of the curve between the metal concentration and time. The metal concentrations were determined by using the Atomic Adsorption Spectrometer (AAS) technique. From the adsorption results, the initial adsorption rates of $Ca^{2+}$ and $Mg^{2+}$ in various systems are shown in Table 4.3.

**Table 4.3** Summary of initial adsorption rates and fractions of ion adsorbed onto the resins in various batch systems.

| Type of system | Adsorption rate*, meq/ml of resin/sec. | Fraction of ion adsorbed onto the resin, % |
|---|---|---|
| $Ca^{2+}$ in single-ion solution | 0.0227 | - |
| $Mg^{2+}$ in single-ion solution | 0.0079 | - |
| $Ca^{2+}$ in mixed-ion solution | 0.0049 | 52.7 |
| $Mg^{2+}$ in mixed-ion solution | 0.0027 | 47.3 |

From batch adsorption experiments, it can be seen that the initial adsorption rates of $Ca^{2+}$ ions both in single-ion solution and mixed-ion solution are much higher than those of $Mg^{2+}$ ions.

* **Method of Adsorption Rate Calculation Shown in Appendix D**

These results clearly demonstrated that the Dowex50-X8 resin has a preferential adsorption of $Ca^{2+}$ ions over the $Mg^{2+}$ ions. Dowex50-X8 resin prefers the higher valence of the exchanging ion and the higher atomic number of the exchanging ion if the valence is constant.

The initial adsorption rate of both $Ca^{2+}$ and $Mg^{2+}$ ions in the single-ion solution is higher than those in the mixed-ion solution (as shown in Figures 4.10 and 4.11) because in the single-ion solution, no competitive ions dissolve in the solution so only one type of ion is adsorbed onto the resin.

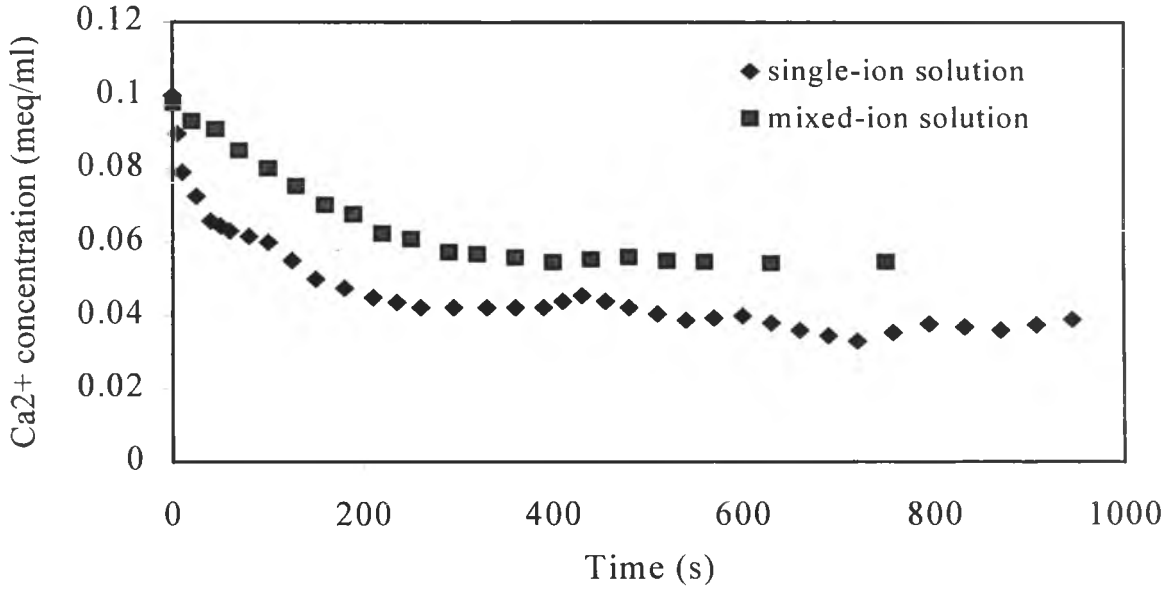


**Figure 4.10** Comparison of adsorption rate of $Ca^{2+}$ ions onto the resin between the single-ion and mixed-ion solutions.

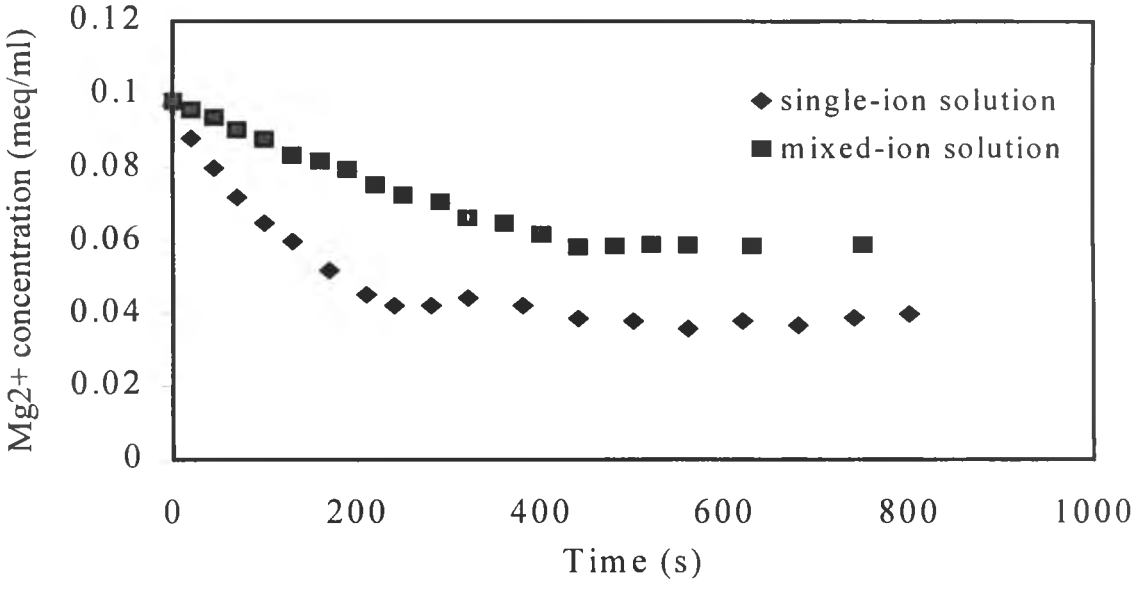


**Figure 4.11** Comparison of adsorption rate of $Mg^{2+}$ ions onto the resin between the single-ion and mixed-ion solutions.

4.5.2 Fixed-Bed Operation

The diagram of steps in determining the fraction of ion adsorbed onto the resins for downflow or fixed-bed operation is also shown in Figure D4. The effect of various flow rates on the adsorption of metal ions from mixed-ion solutions was studied. In addition, the desorption of metal ions from the resin (during regeneration) was also investigated. The adsorption rate can be calculated from the initial slope of the curve of the metal concentration versus time. The fraction of metal ions adsorbed onto the resin can be calculated from the ratio of the adsorption capacity of the resin for particular metal ions (e.g., $Ca^{2+}$) to the total adsorption capacity. This ratio can be determined from the desorption studies (involving regeneration by using HCl). From the adsorption and desorption results, the adsorption rate, the time when the maximum desorption rate occurred and the fraction of ion adsorbed onto the resin in various systems are shown in Tables 4.4 and 4.5.

**Table 4.4** Summary of maximum desorption rate and time at maximum desorption rate for various type of metal ion in mixed-ion solution in fixed-bed operation.

| **Type of ion in mixed-ion solution** | **Maximum desorption rate, meq/ml of resin / sec.** | **Time at maximum desorption rate, sec** |
|---|---|---|
| $Ca^{2+}$ (100 ml/min) | 0.0017 | 160 |
| $Ca^{2+}$ (250 ml/min) | 0.0022 | 35 |
| $Mg^{2+}$ (250 ml/min) | 0.0046 | 10 |

**Same type of ions at different flow rates**. For a higher flow rate of solution, a higher maximum desorption rate was observed because at the higher flow rate, the thickness of the boundary layer, $\delta$, was decreased so the desorption rate was faster. The time when the maximum desorption rate

occurred for higher flow rates of solution is lower than that for lower flow rates because at the higher flow rates there is a higher rate of ion exchange.

**Different type of ions at the same flow rate.** The maximum desorption rate of $Mg^{2+}$ ions is much higher than that of $Ca^{2+}$ ions, indicating that $Mg^{2+}$ ions were easily desorbed from the resin. This can be attributed to the low affinity of the resin towards $Mg^{2+}$ ions as compared to $Ca^{2+}$ ions. The $Mg^{2+}$ ions were less preferred by the resin (due to a lower selectivity value) than $Ca^{2+}$ ions so the $Mg^{2+}$ ions were released from the resin faster than $Ca^{2+}$ ions. The time when the maximum desorption rate occurred for $Mg^{2+}$ ions is also lower than that of $Ca^{2+}$ ions.

**Table 4.5** Summary of average values of fraction of ion in mixed-ion solution adsorbed onto the resins.

| Flow rate of mixed-ion solution, ml/min | Fraction of ion adsorbed onto the resin, % | |
|---|---|---|
| | $Ca^{2+}$ | $Mg^{2+}$ |
| 100 | 63.33 | 36.67 |
| 250 | 71.78 | 28.22 |

The fraction of metal ions adsorbed onto the resin represents equilibrium data or a thermodynamically limited process. The fraction of $Ca^{2+}$ ions adsorbed onto the resin is higher than that of $Mg^{2+}$ ions in both batch (Table 4.3) and fixed-bed (Table 4.5) systems. Again, the reason was the selectivity value (for Dowex50-X8 resin) of $Ca^{2+}$ ions being higher than that of $Mg^{2+}$ ions so the resin prefers more $Ca^{2+}$ ions than $Mg^{2+}$ ions.

The fraction of $Ca^{2+}$ ions adsorbed onto the resin at higher flow rates is higher than that at lower flow rates because at the higher flow rates of solution, the kinetics of the ion exchange has driven the system to a higher equilibrium point.

The steps in the analysis of the results are summarized in Figure 4.12.

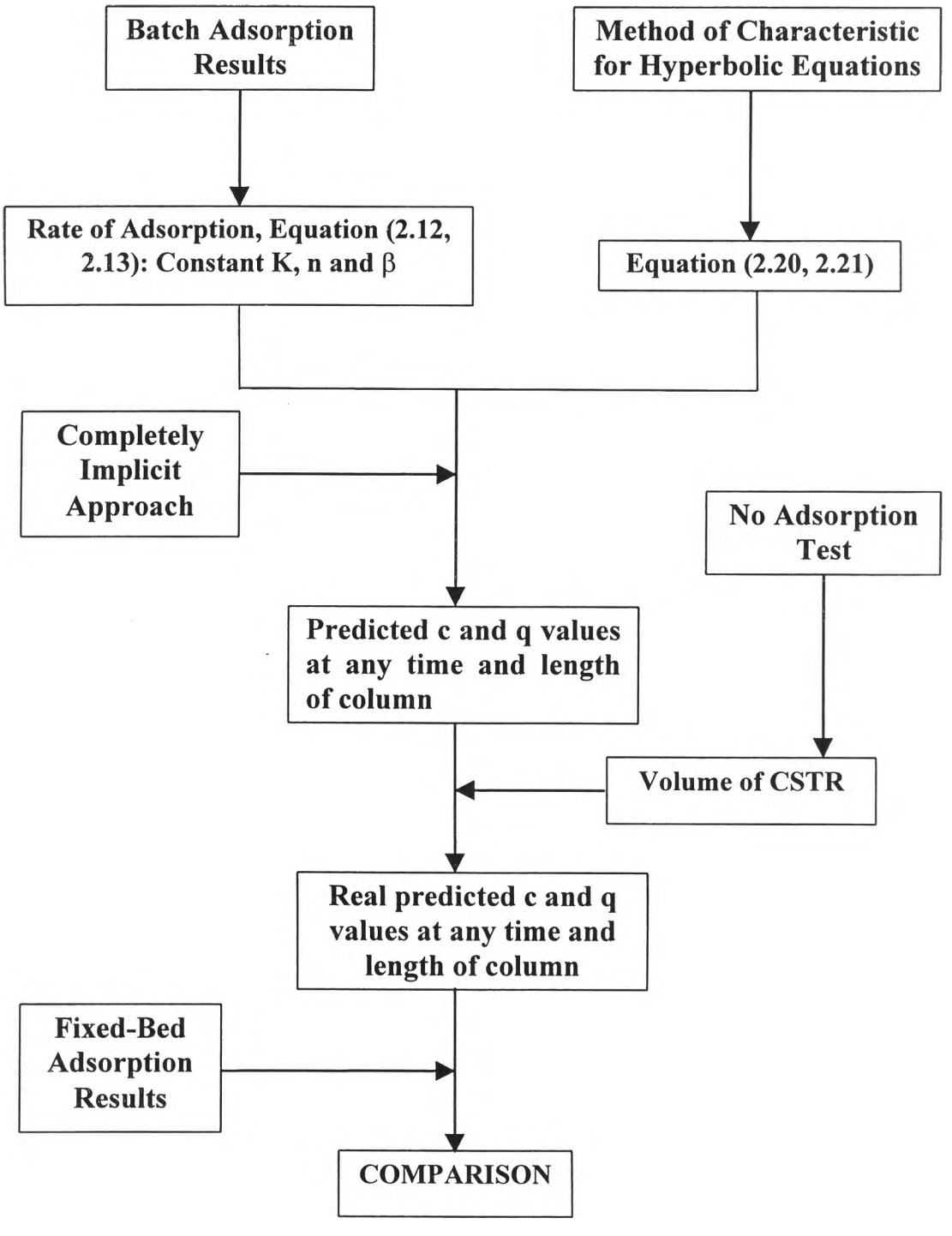


**Figure 4.12** Diagram of mathematical modeling steps for no adsorption test and adsorption of ions in downflow or fixed-bed operation.